A Two-Fluid Model for Vertical Flow Applied to CO_2 Injection Wells

Gaute Linga[a,b], Halvor Lund[a,*]

[a] *SINTEF Energy Research, P.O. Box 4761 Sluppen, NO-7465 Trondheim, Norway*
[b] *Niels Bohr Institute, University of Copenhagen, Blegdamsvej 17, DK-2100 Copenhagen, Denmark*

Abstract

Flow of CO_2 in wells is associated with substantial variations in thermophysical properties downhole, due to the coupled transient processes involved: complex flow patterns, density changes, phase transitions, and heat transfer to and from surroundings. Large temperature variations can lead to thermal stresses and subsequent loss of well integrity, and it is therefore crucial to employ models that can predict this accurately. In this work, we present a model for vertical well flow that includes both two-phase flow and heat conduction. The flow is described by a two-fluid model, where mass transfer between the phases is modelled by relaxation source terms that drive the phases towards thermodynamic equilibrium. We suggest a new formulation of the mass transfer process that satisfies the second law of thermodynamics, and that is also continuous in the single-phase limit. This provides a more robust transition from two-phase to single-phase flow than the previous formulation. The model predicts which flow regimes are present downhole, and calculates friction and heat transfer depending on this. Moreover, the flow model is coupled with a heat conduction model for the layers that comprise the well, including tubing, packer fluid, casing, cement or drilling mud, and rock formation. This enables prediction of the temperature in the well fluid and in each layer of the well. The model is applied to sudden shut-in and blowout cases of a CO_2 injection well, where we employ the highly accurate Span–Wagner reference equation-of-state to describe the thermodynamics of CO_2. We predict pressure, temperature and flow regimes during these cases and discuss implications for well integrity.

Keywords: CO_2 injection wells, two-phase flow, well integrity, thermal modelling

1. Introduction

Carbon Capture and Storage (CCS) will play an important role on the path to a low-carbon society. In the two-degree scenario of the International Energy Agency (IEA), CCS is expected to reduce the global emissions of CO_2 by about seven gigatonnes per year in 2050 [25]. The captured CO_2 can be transported to storage sites using both pipelines and ships. Several authors [3, 27, 55, 68] have concluded that ship transport can be a cost-efficient solution for many offshore storage sites. Ship transport creates additional challenges when CO_2 is injected through a well into a reservoir. The transported CO_2 will typically be kept at a low temperature and pressure, close to the triple point (5.1 bar and −56.6 °C). Some heating will be required before the CO_2 is pumped into the well, in order to avoid damage to the well and the reservoirs due to low temperatures or high pressures. To predict the temperature and pressure conditions in a well, accurate and reliable models are required.

A significant body of research concerns the flow of CO_2 in reservoirs, and leakage through sealed wells [46–48]. The thermal effects of CO_2 flow in reservoirs have also been specifically considered [2, 18]. However, models developed specifically for well flow of CO_2 seem to be scarce, especially for transient scenarios.

For wells without any downhole measuring equipment, steady state models can provide predictions for the pressure and temperature conditions in the well under steady conditions. Lindeberg [32] proposed a simple model using Bernoulli's equation and a model for heat exchange with the surrounding rock, and used it to the predict temperature and

*Corresponding author.
Email addresses: gaute.linga@nbi.ku.dk (Gaute Linga), halvor.lund@sintef.no (Halvor Lund)

pressure in the Sleipner CO_2 injection well. Pan et al. [51] derived an analytic solution for steady-state flow of a CO_2–water mixture in a well using a drift-flux model. Similarly, Lu and Connell [35] proposed a quasi-steady model to predict the bottomhole pressure and injection rate in a CO_2 injection well. Singhe et al. [59] presented a simple quasi-steady analytical model for temperature effects in a gas injection well, and compared their model to results from the Ketzin injection well [24]. Han et al. [22] considered injection of relatively hot (supercritical) CO_2 at 35 °C to 45 °C, using a model based on that of Lu and Connell [35]. They focused on the effects of CO_2 injection on injectivity, due to cooling when water vaporizes in supercritical CO_2, and the following precipitation of salt. Precipitation of salt has been identified as one of the main causes of the pressure build-up experienced during CO_2 injection at Snøhvit [23].

Transient models allow the prediction of conditions in wells that are subject to more transient operations such as blowout, shut-in and varying injection rates. Ruan et al. [56] considered an axisymmetric two-dimensional model, accounting for the convection of water in the annulus in addition to that of the CO_2 in the tubing. They simulated injection using the Peng–Robinson cubic equation of state with a reservoir pressure of 27 MPa, which resulted in the CO_2 being in a single, dense phase during the injection scenario. Pan et al. [50] implemented a drift-flux model in the TOUGH2 code with the ECO2N equation of state, and used it to simulate upwards flow of CO_2 and brine in a wellbore. Lu and Connell [37] simulated CO_2 injection using the homogeneous equilibrium model and the Peng–Robinson cubic equation of state, coupled with a heat conduction model. The same authors have also presented a drift-flux model with phase slip [36].

Krogh et al. [29] simulated offloading of CO_2 from ships and injection of liquid CO_2 using OLGA and HYSYS. They found that there is a high risk of hydrate formation and freezing in the formation and on the outside of the riser. Klinkby et al. [28] also used OLGA to study transient variations in pressure, temperature and phase composition during injection of CO_2–brine mixtures into the proposed Vedsted pipeline, injection well, and reservoir. Li et al. [31] focused on the well-head temperature during shut-in and start-up, also using OLGA. Azaroual et al. [4] presented experiments and modelling of injection of supercritical CO_2 into saline aquifers. They focused on how e.g. precipitation of salt due to dryout in the near wellbore can lead to changes in injectivity. Three commercial simulators – PipeSIM, PROSPER and NEWSIM – were used and their results compared, which showed significant differences.

The available research on flow in vertical CO_2 wells is to a large extent based on either simplified steady-state models, or commercial simulators. The use of complex commercial simulators can make model validation difficult, since there is often little public data available about the details of the models.

1.1. Contributions of the current paper

In this paper, we aim to present a model that is suitable for vertical flow of CO_2, and to explain to a sufficient level of detail all parameters and submodels used. The flow is described by a physically consistent two-fluid model, with the Span–Wagner reference equation-of-state [61] to describe the thermodynamics of CO_2. Friction and heat transfer in the flow is modelled specifically for each flow regime, such as bubbly, annular and mist flow. The flow model is coupled to a model for heat conduction through the various layers of the well, such as tubing, packer fluid, casing, cement and rock. Large temperature variations can be detrimental to well integrity and are therefore given special attention. The performance of the model is demonstrated by using it to simulate transient well operations; in particular critical incidents such as sudden shut-in and blowout.

1.2. Paper outline

In Section 2, we present the model including flow equations, heat conduction model and correlations employed for friction and fluid-to-wall heat transfer. Section 3 gives a brief description of the numerical methods used, with references to relevant literature, and Section 4 presents the simulation cases considered. In Section 5 we present results from simulations of sudden blowout and shut-in of a vertical CO_2 well, with emphasis on pressure and temperature conditions in the well. We also discuss the implications of the simulation results on well operations and well integrity. Finally, in Section 6, we summarize and draw conclusions.

2. Model

In this section, we present the model used in our simulations.

2.1. Flow model

In the present work, we consider pure CO_2 in at most two phases, i.e. liquid and gas. Since the vertical length scale of a well is several orders of magnitude larger than the radial scale, we consider a fluid flowing in one dimension. Modelling the flow in more than one dimension could require detailed resolution of the gas–liquid interface, as well as a much higher computational cost. For this reason, most models for well and pipeline flow are one-dimensional, with constitutive relations that implicitly account for higher-dimensional effects that cannot be explicitly captured in a one-dimensional model.

In order to allow for three-dimensional effects, such as phase separation, we employ a *two-fluid model*. This class of two-phase flow models is characterized by the property that the two phases are allowed to have individual velocities, i.e. each phase is governed by a separate momentum equation [44, 49, 62, 67]. This is in contrast to the further simplified class of drift-flux models [16, 41, 58, 69], wherein the velocities of the two phases are related by a functional relation (a slip law).

Two-fluid models have been extensively studied in the literature, and are commonly used in numerous applications. A general seven-equation model for two-phase flow was derived by Baer and Nunziato [5], and later revived by Saurel and Abgrall [57], upon which many of later two-phase flow models have been based. To bring the phases towards equilibrium in velocity, pressure, temperature or specific Gibbs free energy at a finite rate, relaxation source terms are typically included in the equations of motion. This has been studied by a range of authors [6, 26, 45, 52, 53]. By assuming instantaneous equilibrium, i.e. infinitely stiff relaxation source terms, in zero or more of these variables, a hierarchy of models can be derived [15, 33, 38]. For each imposed equilibrium condition, the number of partial differential equations (PDEs) in the model is reduced by one. Popular models in this context include e.g. a six-equation two-fluid model used in nuclear industry [8, 66], and a five-equation model used in simulation of pipeline transport of petroleum [7].

For the purpose of our simulations, we assume that the time scale of the thermodynamic relaxation is much smaller than that of the flow, and hence we assume instantaneous equilibrium in pressure (p), temperature (T) and specific Gibbs free energy (μ). However, for practical reasons (which we shall discuss in Section 2.2), we choose to allow the specific Gibbs free energy to be out of equilibrium and model mass transfer using a relaxation process. The resulting five-equation two-fluid model (the pT-model, cf. [33]) was studied by Martínez Ferrer et al. [40] and further by Morin and Flåtten [42]. Hammer and Morin [20] combined the model with the Span–Wagner equation of state [61].

With source terms accounting for the interaction between phases and with the pipe wall, the model may be stated as the following set of PDEs, for time t and spatial coordinate x,

- Mass balance:

$$\partial_t(\alpha_{\mathrm{g}}\rho_{\mathrm{g}}) + \partial_x(\alpha_{\mathrm{g}}\rho_{\mathrm{g}}v_{\mathrm{g}}) = \Psi, \tag{1}$$
$$\partial_t(\alpha_{\ell}\rho_{\ell}) + \partial_x(\alpha_{\ell}\rho_{\ell}v_{\ell}) = -\Psi, \tag{2}$$

- Momentum balance:

$$\partial_t(\alpha_{\mathrm{g}}\rho_{\mathrm{g}}v_{\mathrm{g}}) + \partial_x\left(\alpha_{\mathrm{g}}(\rho_{\mathrm{g}}v_{\mathrm{g}}^2 + p)\right) - p_{\mathrm{i}}\partial_x\alpha_{\mathrm{g}} = v_{\mathrm{i}}\Psi + f_{\mathrm{i}} + \alpha_{\mathrm{g}}\rho_{\mathrm{g}}g_x - f_{\mathrm{wall,g}}, \tag{3}$$

$$\partial_t(\alpha_{\ell}\rho_{\ell}v_{\ell}) + \partial_x\left(\alpha_{\ell}(\rho_{\ell}v_{\ell}^2 + p)\right) + p_{\mathrm{i}}\partial_x\alpha_{\mathrm{g}} = -v_{\mathrm{i}}\Psi - f_{\mathrm{i}} + \alpha_{\ell}\rho_{\ell}g_x - f_{\mathrm{wall},\ell}, \tag{4}$$

- Energy conservation:

$$\partial_t E + \partial_x\left(E_{\mathrm{g}}v_{\mathrm{g}} + E_{\ell}v_{\ell} + \bar{v}p\right) = (\alpha_{\mathrm{g}}\rho_{\mathrm{g}}v_{\mathrm{g}} + \alpha_{\ell}\rho_{\ell}v_{\ell})g_x + Q. \tag{5}$$

Herein, we have used the volume fraction α_k, the density ρ_k, and the velocity v_k for each phase $k \in \{\mathrm{g}, \ell\}$, where g denotes gas and ℓ denotes liquid. We have defined the total phasic energy by

$$E_k = \alpha_k\rho_k\left(e_k + \tfrac{1}{2}v_k^2\right), \tag{6}$$

where e_k is the specific internal energy. The common pressure is denoted by p, the mixed density and mixed total energy are respectively given by

$$\rho = \alpha_{\mathrm{g}}\rho_{\mathrm{g}} + \alpha_{\ell}\rho_{\ell}, \quad \text{and} \quad E = E_{\mathrm{g}} + E_{\ell}, \tag{7}$$

and the volume-averaged velocity is given by

$$\bar{v} = \alpha_\mathrm{g} v_\mathrm{g} + \alpha_\ell v_\ell. \tag{8}$$

The regularizing interface pressure, which makes the model hyperbolic, is modelled as [64]

$$p_\mathrm{i} = p - \delta \frac{\alpha_\mathrm{g}\alpha_\ell\rho_\mathrm{g}\rho_\ell}{\alpha_\ell\rho_\mathrm{g} + \alpha_\mathrm{g}\rho_\ell}(v_\mathrm{g} - v_\ell)^2, \tag{9}$$

where $\delta \geq 1$, and in this work we choose $\delta = 1.2$. Further, f_i is an interfacial friction term, g_x is the gravitational acceleration along the x coordinate, $f_{\mathrm{wall},k}$ represents the fluid–wall friction of phase k, and Q represents heat exchange with the surroundings. Finally, Ψ represents the mass transfer between the two phases, and v_i is the interfacial velocity. Expressions for these terms will be given in the following.

2.2. Mass transfer

The term Ψ, representing mass transfer between phases, can in general be expressed as $\Psi = \mathcal{K}(\mu_\ell - \mu_\mathrm{g})$, where $\mathcal{K}$ is associated with a characteristic *relaxation* time for the mass transfer. As $\mathcal{K} > 0$, the relaxation term drives the two phases asymptotically towards equilibrium in specific Gibbs free energy, i.e. mass is transferred from the phase with the highest Gibbs free energy to the phase with the lowest, until the values are equal. If the mass transfer is taken to be instantaneous (as advocated in the previous section), i.e. $\mathcal{K} \to \infty$ (zero relaxation time), the model is equivalent to the four-equation model with full thermodynamic equilibrium [20], as described by Morin and Flåtten [42]. In particular, solutions of the relaxation model should approach solutions to the equilibrium model as $\mathcal{K} \to \infty$. For a recent survey of the underlying theory for general hyperbolic relaxation systems, consider Solem et al. [60, Sec. 1] and the references therein.

Mass transfer also leads to transfer of momentum, represented by the term $v_\mathrm{i}\Psi$ in eqs. (3) and (4). As Morin and Flåtten [42] point out, $v_\mathrm{i} = (v_\mathrm{g} + v_\ell)/2$ is the only interfacial velocity that satisfies the second law of thermodynamics (i.e. that the global entropy is nondecreasing), and that is also independent of the difference in specific Gibbs free energy $\mu_\mathrm{g} - \mu_\ell$.

The relation between change in entropy and in kinetic energy, when transferring mass from one phase to the other, is found from the fundamental thermodynamic relation,

$$\mathrm{d}(\rho e) = T\,\mathrm{d}S + \mu\,\mathrm{d}\rho = T\,\mathrm{d}S, \tag{10}$$

where have utilized that the total mass is constant, $\mathrm{d}\rho = 0$, and introduced the total volumetric entropy S and the mixture specific Gibbs free energy $\mu = e + (p - TS)/\rho$. The total energy $E = \rho e + E_\mathrm{kin}$ is conserved,

$$\mathrm{d}E = \mathrm{d}(\rho e) + \mathrm{d}E_\mathrm{kin} = 0. \tag{11}$$

Combining eqs. (10) and (11) yields

$$\mathrm{d}S = -\frac{1}{T}\,\mathrm{d}E_\mathrm{kin}, \tag{12}$$

in other words the second law of thermodynamics, implied by the local relation $\mathrm{d}S \geq 0$ [15, 33, 38, 42], is satisfied as long as the kinetic energy is not increasing during the mass transfer process. Note that these relations only apply to the *local* mass transfer process, not the fluid flow model as a whole.

The interfacial velocity suggested by Morin and Flåtten [42] conserves kinetic energy during the mass transfer relaxation process, and, in other words, no entropy is generated. However, this interfacial velocity presents problems if the mass transfer process brings us from a two-phase to a single-phase solution. In this case, kinetic energy cannot be conserved and entropy must be generated, as we will see next.

We will solve the equation system (1)–(5) using a fractional-step method, in which we

1. solve the equation (1)–(5) system with $\Psi = 0$,
2. solve an ODE system for mass transfer given by

$$\frac{\mathrm{d}M_\mathrm{g}}{\mathrm{d}t} = \Psi, \tag{13}$$

$$\frac{\mathrm{d}M_\ell}{\mathrm{d}t} = -\Psi, \tag{14}$$

$$\frac{\mathrm{d}\Pi_\mathrm{g}}{\mathrm{d}t} = v_\mathrm{i}\Psi, \tag{15}$$

$$\frac{\mathrm{d}\Pi_\ell}{\mathrm{d}t} = -v_\mathrm{i}\Psi, \tag{16}$$

$$\frac{\mathrm{d}E}{\mathrm{d}t} = 0, \tag{17}$$

where we have introduced the shorthands $M_k \equiv \alpha_k\rho_k$ and $\Pi_k \equiv \alpha_k\rho_k v_k$ for mass and momentum of phase k, respectively. The mass transfer term is $\Psi = \mathcal{K}(\mu_\ell - \mu_\mathrm{g})$ where $\mathcal{K} \to \infty$, so the ODE system approaches thermodynamic equilibrium where

$\mu_{\mathrm{g}} = \mu_\ell$. We therefore rather solve a more straightforward discrete equation system.

Let M_k^* and Π_k^* denote the mass and momentum of phase k after the homogeneous step (step 1), and M_k and Π_k denote values after mass has been transferred (step 2). We need to conserve total mass, momentum and energy,

$$\sum_k M_k^* = \sum_k M_k \tag{18}$$

$$\sum_k \Pi_k^* = \sum_k \Pi_k \tag{19}$$

$$\sum_k M_k^* \left(e_k^* + \frac{1}{2}(v_k^*)^2\right) = \sum_k M_k \left(e_k + \frac{1}{2}v_k^2\right) \tag{20}$$

Through the equation of state we ensure thermodynamic equilibrium,

$$\mu_{\mathrm{g}}(e_{\mathrm{g}}, \rho_{\mathrm{g}}) = \mu_\ell(e_\ell, \rho_\ell) \tag{21}$$

$$p_{\mathrm{g}}(e_{\mathrm{g}}, \rho_{\mathrm{g}}) = p_\ell(e_\ell, \rho_\ell) \tag{22}$$

$$T_{\mathrm{g}}(e_{\mathrm{g}}, \rho_{\mathrm{g}}) = T_\ell(e_\ell, \rho_\ell) \tag{23}$$

Together with $\sum_k \alpha_k = 1$, this gives us 7 equations and 8 unknowns (α_k, e_k, ρ_k, v_k), which allows us to make a choice that determines the amount of entropy generated by the mass transfer, or in other words how much kinetic energy is lost.

However, if the equation of state predicts that the mass transfer will lead to a single-phase solution, we are forced to set $\alpha_V = v_V = 0$, where V is the vanishing phase. Interestingly, this uniquely determines the total kinetic energy after the mass transfer,

$$E_{\mathrm{kin}} = \frac{1}{2} M_K v_K^2 = \frac{(\sum_k \Pi_k^*)^2}{2\sum_k M_k^*}, \tag{24}$$

where K is the phase that is kept. The change in kinetic energy is given by

$$\begin{aligned}\Delta E_{\mathrm{kin}} &= \frac{1}{2}\left[\frac{(\sum_k \Pi_k^*)^2}{\sum_k M_k^*} - \sum_k M_k^* (v_k^*)^2\right] \\ &= -\frac{M_{\mathrm{g}}^* M_\ell^*}{2\rho}(v_{\mathrm{g}}^* - v_\ell^*)^2\end{aligned} \tag{25}$$

As we see, kinetic energy is lost, which corresponds to an increase in entropy as given by eq. (12). With this insight, we therefore suggest a general expression for the kinetic energy lost,

$$\begin{aligned}\Delta E_{\mathrm{kin}} = &-\frac{1}{2}(M_{\mathrm{g}}^*(\Delta v_{\mathrm{g}}^*)^2 + M_\ell^*(\Delta v_\ell^*)^2) \\ &\cdot \left(\frac{|M_{\mathrm{g}} - M_{\mathrm{g}}^*|}{\rho - |M_{\mathrm{g}} + M_{\mathrm{g}}^* - \rho|}\right),\end{aligned} \tag{26}$$

where $\Delta v_k^* \equiv v_k^* - \hat{v}^*$, and

$$\hat{v}^* = (\Pi_{\mathrm{g}}^* + \Pi_\ell^*)/\rho, \tag{27}$$

is the centre-of-mass velocity. This expression (26) gives a smooth transition between cases where kinetic energy must be lost, and those where it can be conserved. For example, $\Delta E_{\mathrm{kin}} = 0$ if the velocities are equal or if no mass is transferred, while eq. (25) is fulfilled if $M_{\mathrm{g}} = 0$ or $M_\ell = 0$. We propose that this gives a numerically more robust transition from two-phase to single-phase flow than the previous formulation, which we experienced to give unphysical oscillations in the transition region.

2.3. Equation of state

The state-of-the-art reference equation-of-state (EOS) for CO_2 is that of Span and Wagner [61], which gives the Helmholtz free energy in terms of phasic density and temperature, i.e. $a(\rho, T)$. It is formulated in terms of the non-dimensional Helmholtz free energy $\phi = a/RT$, where R is the specific gas constant; and is comprised of an ideal gas part, ϕ^0, and a residual part, ϕ^{r},

$$\phi(\tau, \delta) = \phi^0(\tau, \delta) + \phi^{\mathrm{r}}(\tau, \delta). \tag{28}$$

Here, $\tau = T_{\mathrm{c}}/T$ is the non-dimensional inverse temperature, and $\delta = \rho/\rho_{\mathrm{c}}$ is the non-dimensional density. ρ_{c} and T_{c} are the critical density and temperature, respectively. The expressions in the original paper [61] contain a total of 51 terms, including logarithms and exponentials, making it computationally demanding to solve compared to e.g. cubic equations of state. However, due to their simplicity, cubic equations of state do not accurately describe the thermophysical properties of CO_2 on the vast range of densities and temperatures required for simulating CO_2 injection wells, in contrast to the Span–Wagner EOS. The energy–density equilibrium problem is solved using the approach of Hammer et al. [21].

2.4. Flow regimes

The behaviour of two-phase flow can change dramatically depending on the amount of gas in the flow and the velocity of each phase. This behaviour can typically be divided into flow regimes, such as bubbly, stratified, slug, churn, annular and dispersed/mist flow.

Since experimental data and mathematical models for flow regimes in vertical CO_2 flow are rather

scarce, we use the RELAP [54] code to classify flow regimes. RELAP was developed for simulation of water–steam flow in cooling systems for nuclear reactors. Nevertheless, its expressions for flow regimes and friction are formulated so that the properties of any fluid can be used as input, which allows us to use them for CO_2 flow. We limit ourselves to bubbly, annular and mist flow, since these flow regimes are most relevant for the cases we look at. Slug flow is not expected to occur in vertical pipes of such large diameters as those we consider; in the RELAP code the maximum diameter where slug flow can occur is 8 cm.

2.5. Friction

The friction correlations we have employed are based on the RELAP code [54]. Since experimental data on CO_2 in large-diameter tubes are scarce, we assume that RELAP's correlations hold also for CO_2, as long as physical parameters for CO_2 are used as input.

2.6. Heat transfer

Heat transfer between the fluid and the pipe wall can depend significantly on which flow regime is present. For turbulent flow we use the correlation by Dittus and Boelter [13]. For subcooled and saturated boiling, we use the correlations by Chen [12] and Forster and Zuber [17].

2.7. Heat conduction

Heat conduction is modelled in the layers extending outwards from the well tubing. In a radial geometry this can be expressed as [10]

$$\rho(r)c_p(r)\partial_t T(r,t) = \frac{1}{r}\partial_r\left(r\kappa(r)\partial_r T(r,t)\right), \quad (29)$$

where $\kappa(r)$, $\rho(r)$ and $c_p(r)$ are the thermal conductivity, density and specific heat capacity (at constant pressure) at radius r, respectively. Using this formulation, we neglect any heat conducted along the pipe (in the axial direction). Heat is nevertheless transported along the pipe by the fluid inside the well.

3. Numerical method

In this section, we present the numerical methods used in the simulations. We may write the equation system (1)–(5) as

$$\partial_t \mathbf{u} + \partial_x \mathbf{f}(\mathbf{u}) + \mathbf{B}(\mathbf{u})\partial_x \mathbf{w}(\mathbf{u}) = \mathbf{s}(\mathbf{u}). \quad (30)$$

In general terms, we can write eq. (30) as

$$\partial_t \mathbf{u} = (\mathcal{A} + \mathcal{B})\mathbf{u}, \quad (31)$$

where $\mathcal{A}$ and $\mathcal{B}$ are the solution operators for the flow and source terms, respectively. If $\mathbf{u}^n$ is the solution at time t^n, then the solution $\mathbf{u}^{n+1}$ at time $t^{n+1} = t^n + \Delta t$ can be formally written as [30]

$$\mathbf{u}^{n+1} = \mathrm{e}^{\Delta t(\mathcal{A}+\mathcal{B})}\mathbf{u}^n \quad (32)$$

Since the flow and source terms have somewhat different time scales, we treat them separately using a fractional-step approach. A fractional-step approach applies the solution operators in separate steps, as opposed to simultaneously. Strang splitting [63] is a second-order fractional-step method, as long as each step is of second order, and applies the operators in three steps,

$$\mathbf{u}^{n+1} = \mathrm{e}^{\Delta t/2\mathcal{B}}\mathrm{e}^{\Delta t\mathcal{A}}\mathrm{e}^{\Delta t/2\mathcal{B}}\mathbf{u}^n \quad (33)$$

In other words, we first apply flux terms with time step $\Delta t/2$, then the source terms with time step Δt, and finally flux terms again. This splitting allows us to solve each substep in the most efficient way. In the following, we describe how each substep is solved.

3.1. Flow equations

The flow equations

$$\partial_t \mathbf{u} + \partial_x \mathbf{f}(\mathbf{u}) + \mathbf{B}(\mathbf{u})\partial_x \mathbf{w}(\mathbf{u}) = 0, \quad (34)$$

are solved with a finite-volume scheme. To achieve second spatial order, we use piecewise linear reconstruction based on the MUSCL approach, and use the FORCE flux to calculate the numerical fluxes. For more details, see Hammer and Morin [20].

A main advantage of employing a finite-volume scheme is that conserved quantities are well conserved over shocks, not only for smooth solutions. However, such numerical schemes generally apply to the flux part ($\partial_x \mathbf{f}$) of eq. (34), and the non-conservative part ($\mathbf{B}\partial_x \mathbf{w}$) must be integrated separately, e.g. as a source term. In our context, this affects only the numerical integration of the momentum eqs. (3) and (4).

An important property that should be satisfied, is therefore that the *total* momentum should be conserved (up to the accuracy of the finite-volume scheme), according to its evolution equation, which is found by summing eqs. (3) and (4):

$$\partial_t \Pi + \partial_x\left(\Pi_\mathrm{g} v_\mathrm{g} + \Pi_\ell v_\ell + p\right) = 0. \quad (35)$$

Here we disregard wall friction, gravity and heat transfer for the sake of the argument, and $\Pi \equiv \Pi_g + \Pi_\ell$ is the total momentum. In order to conserve the total momentum, summing the discretizations of eqs. (3) and (4), the numerical scheme should therefore reduce to a pure flux formulation,

$$\partial_t \Pi_i = (F_{i-1/2} - F_{i+1/2})/\Delta x. \quad (36)$$

In the model formulation of Hammer and Morin [20], the momentum equations are discretized as

$$\partial_t \Pi_{g,i} = (F_{g,i-1/2} - F_{g,i+1/2} + \alpha_g \Delta p_i)/\Delta x, \quad (37)$$
$$\partial_t \Pi_{\ell,i} = (F_{\ell,i-1/2} - F_{\ell,i+1/2} + \alpha_\ell \Delta p_i)/\Delta x, \quad (38)$$

which yields the total momentum discretization

$$\partial_t \Pi_i = (F_{\ell,i-1/2} - F_{\ell,i+1/2} + F_{g,i-1/2} - F_{g,i+1/2} + \Delta p_i)/\Delta x. \quad (39)$$

The superfluous last term in eq. (39), with respect to eq. (36), shows that this formulation does not conserve total momentum properly. In the present model formulation, i.e. eqs. (3) and (4), we have

$$\partial_t \Pi_{g,i} = (F_{g,i-1/2} - F_{g,i+1/2} + p_i \Delta \alpha_{g,i})/\Delta x, \quad (40)$$
$$\partial_t \Pi_{\ell,i} = (F_{\ell,i-1/2} - F_{\ell,i+1/2} + p_i \Delta \alpha_{\ell,i})/\Delta x, \quad (41)$$

which adds up to

$$\partial_t \Pi_i = (F_{\ell,i-1/2} - F_{\ell,i+1/2} + F_{g,i-1/2} - F_{g,i+1/2})/\Delta x. \quad (42)$$

Identifying $F_{i\pm1/2} = F_{g,i\pm1/2} + F_{\ell,i\pm1/2}$, this complies with eq. (36). In other words, our model formulation ensures that whatever amount of momentum is added to one phase due to non-conservative terms, is subtracted from the other phase. Hence, the total momentum is conserved according to eq. (35), up to the accuracy of the flux-based numerical scheme.

3.2. Source terms and closure relations

The source term ODEs

$$\frac{\mathrm{d}\mathbf{u}}{\mathrm{d}t} = \mathbf{s}(\mathbf{u}), \quad (43)$$

are solved using the Forward Euler method. Since we let the flow equations determine the global time step Δt, it might need to be reduced to ensure stability in the source terms ODE. In this case, more than one smaller time step Δt_s is performed that in total add up to Δt.

3.3. Heat equations

The heat equation (29) is solved using a finite volume scheme as described by Lund et al. [39].

3.4. Reservoir boundary condition

The injection rate into a reservoir can be described by the *injectivity* I, which determines the injection rate resulting from a certain pressure difference between the well and the reservoir. This is implemented as a ghost cell with prescribed pressure $p = p_{\text{reservoir}} + (A\rho\hat{v})/I$ where $A\rho\hat{v}$ is the flow rate. The same procedure is used when fluid flows *out* of the reservoir, in which case the pressure in the well will be lower than the reservoir pressure. In other words we assume that the productivity and injectivity are equal.

4. Simulation cases

In the following, we describe the simulation cases including material parameters, initial and boundary conditions. In all cases, we use the same well geometry and material parameters. Key parameters are listed in Table 1. The parameters used are inspired by the conditions at the Sleipner CO_2 injection well [29, 32], and hence the results are to some extent applicable to this well. However, in our case we consider a purely vertical well of length 1000 m, whereas the Sleipner well has significant horizontal deviation. In a real-world application, the reservoir injectivity/productivity will typically be time-dependent when the well starts to produce. However, since the effect of injectivity is not our main focus, we here assume a constant reservoir injectivity.

The heat conduction model assumes that the well is divided into five layers, whose properties are listed in Table 2. The layers are a 7 inch tubing, packer fluid, 9.5 inch casing, drilling mud (or cement for the lower 100 meters), and a sandstone formation.

4.1. Sudden blowout

In this case, we consider an abrupt blowout scenario from a well. In the initial state, the well is closed at the top, and in contact with the reservoir at the bottom. The initial condition consists of a column of liquid in the lower part of the well, and gas in the upper part of the well. The pressure is assumed to be hydrostatic, extrapolated from the reservoir pressure in the bottom of the well. The

Table 1: Well and reservoir properties used in simulations.

Parameter	Value	Unit	Reference
Well depth	1000	m	[29, 32]
Ambient water temperature	5	°C	[29]
Geothermal gradient	41	°C/km	[32]
Reservoir pressure	104	bar	[32]
Injectivity/Productivity	8.7×10^{-5}	kg/(s Pa)	[65]

Table 2: Material properties and dimensions for the layers surrounding the pipe.

Item	Radial segment [cm]	Axial segment [km]	Density [kg/m^3]	Thermal conductivity [W/(m K)]	Specific heat capacity [J/(kg K)]
Tubing (ST 52-3) [1]	8.5–9.0	0–1	7850	40	500
Packer fluid [19]	9.0–11.1	0–1	1400	0.26	4000
Casing (ST 52-3) [1]	11.1–12.2	0–1	7850	40	500
Drilling mud [9]	12.2–15.5	0–0.9	1500	0.8	2500
Cement (Portland Class G) [1]	12.2–15.5	0.9–1	1917	0.72	780
Sandstone (Castlegate) [1]	15.5–500	0–1	2600	2.0	1000

temperature is assumed to be equal to the rock temperature until the boiling point is reached (at around 250 m depth), above which the temperature is set to be slightly above the boiling point, so that the fluid is in a gas state. The initial condition is illustrated in Figure 1.

At $t = 0$, the well head is opened to atmospheric pressure, $p = 1.013$ bar. If the flow reaches sonic velocities, the flow is choked (see e.g. [34]) by imposing the choke pressure at the outlet, rather than the atmospheric pressure [43]. The lower end of the well is in contact with the reservoir, as described in Section 3.4, which causes CO_2 to flow from the reservoir into the well.

4.2. Sudden shut-in

In the shut-in case, we assume that there is a steady injection of CO_2 into the reservoir in the initial condition. The flow is set to 28.7 kg/s, similar to the flow in the Sleipner well [65]. The bottom temperature is set to the reservoir temperature, and the pressure is set according to Section 3.4. The pressure in the rest of the well is set so that it balances the friction and gravity forces,

$$\partial_x p = f_{\text{grav}} - f_{\text{wall}}. \tag{44}$$

The temperature is set by assuming the flow is isentropic, which leads to the initial condition depicted in Figure 2. At $t = 0$, valves at both ends of the pipe are abruptly closed.

It turns out that the resulting initial well-head conditions are rather close to those present at Sleipner. The pressure and temperature at the Sleipner well-head are known to be 65 bar and 24 °C, whereas the gas fraction has been estimated to be around 0.85 [65].

5. Results and discussion

5.1. Blowout

The blowout case was simulated for 150 s, after which a somewhat steady flow out of the reservoir was reached. Figure 3 shows the pressure at three locations in the pipe. The pressure at the outlet drops rapidly from 60 bar to approximately 10 bar in the first seconds, before it increases somewhat around $t = 7$ s. At this time, the speed of sound suddenly drops, since flow changes from pure gas to a two-phase mixture, as seen in Figure 4. This causes the flow to be choked, resulting in a pressure jump. The pressure in the bottom part of the well drops slowly as the flow out of the reservoir increases, as specified in Section 3.4.

Figure 4 shows the gas volume fraction for the well head and the middle of the well. A small amount of liquid occurs at the well head in early phases of the blowout, which is likely to have been

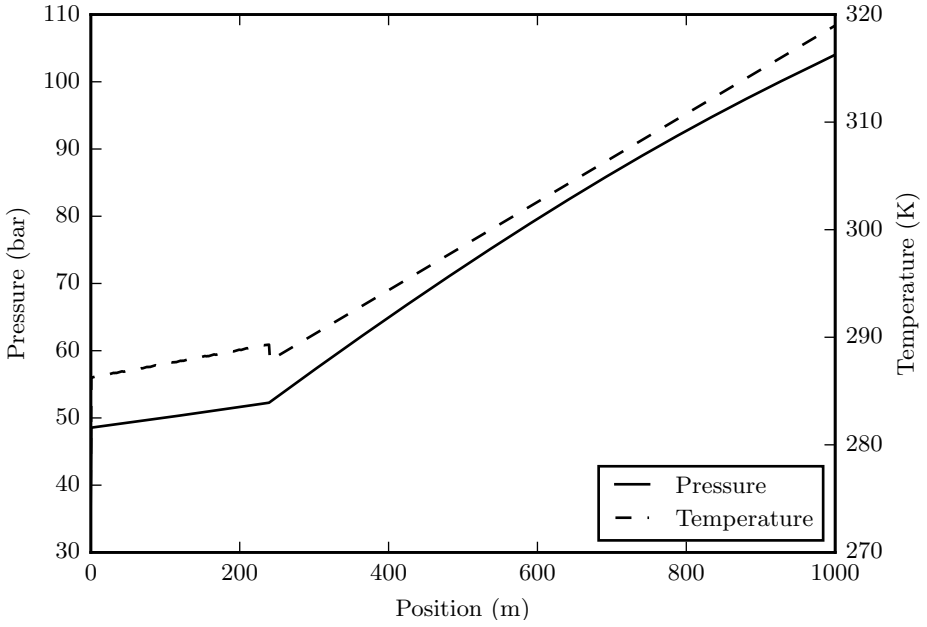

Figure 1: Initial condition before blowout. There is liquid below $x \approx 250\,\mathrm{m}$, and gas above.

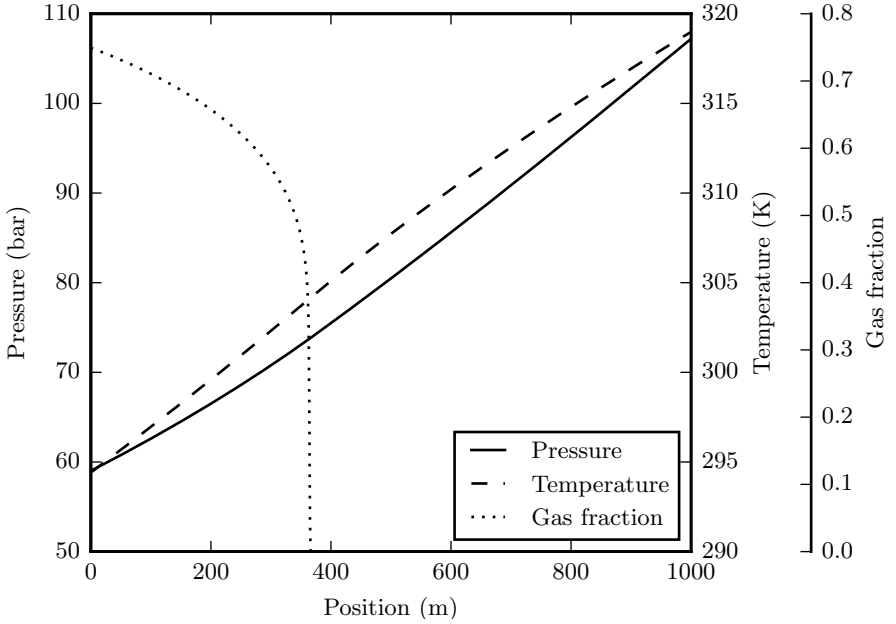

Figure 2: Initial condition before shut-in.

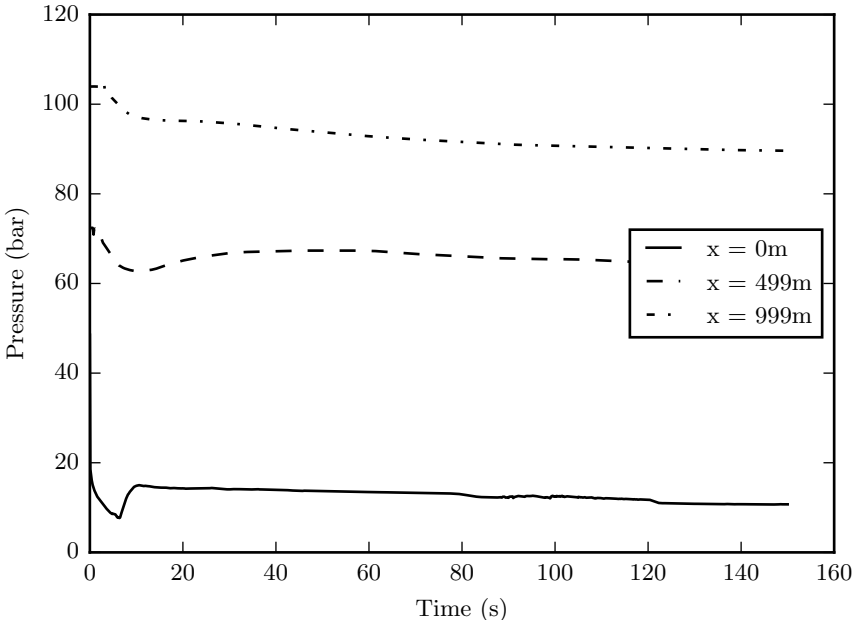

Figure 3: Pressure during blowout for three pipe locations.

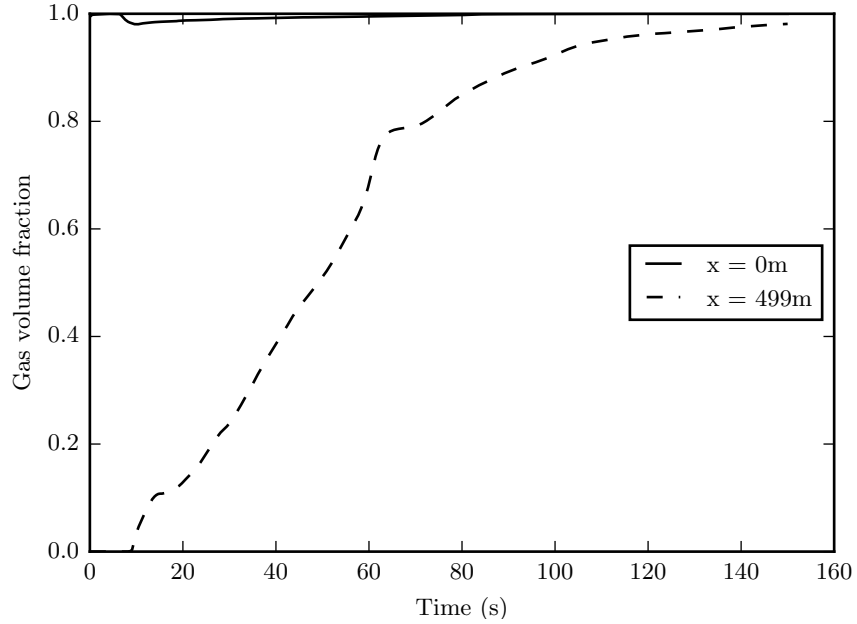

Figure 4: Gas volume fraction during blowout at the well head and in the middle of the well.

sucked up from the liquid column due to the rapid flow of gas. The middle of the well transitions gradually from pure liquid to almost pure gas over the course of the simulation, as the pressure slowly drops.

Figure 5 shows the flow regimes present in each part of the well. In the initial condition, the whole well is in a single-phase state (either pure liquid or pure gas). During the first 50–55 seconds, the upper part of the liquid column quickly boils and creates a zone of bubbly flow. When the velocity has increased sufficiently, most of the upper well has annular flow, with a liquid annulus and gas flowing in the middle. After around 100 seconds, the flow at the well head is purely gaseous.

During blowouts, very low temperatures can occur, which can be detrimental to well integrity and materials. Figure 6 shows the temperature at three well locations. Since the flow in the bottom of the well comes directly from the reservoir, which has a temperature of 319 K, the lower part of the well does not experience any significant temperature drop. At the well head, however, temperatures as low as 225 K (or −48 °C) occur in the initial phase. The well head temperature rises somewhat when the flow is choked after around 7 seconds, and is thereafter steady at around 240 K (or −33 °C). This temperature is not necessarily low enough to cause damage to the steel pipe itself, but may be problematic due to mechanical stresses that arise due to thermal contraction.

It is important to note that our simulations do not predict any formation of dry ice in the well itself, although it might be formed just beyond the outlet at the well head. However, we assume that the temperature of the flow out of the reservoir is equal to the long-scale reservoir temperature. This is unlikely to hold on longer time scales, since some Joule–Thomson cooling will occur as the CO_2 fluid flows through the pores of the reservoirs and out into the well. The prediction of this phenomenon will require coupling the flow model to a reservoir model. Over time, the temperature of the flow from the reservoir will likely decrease, potentially damaging the well and allowing dry ice to form.

5.2. Shut-in

The shut-in case is simulated for around 40 seconds, which allows us to capture the most important features of the initial phase of a shut-in. Since valves are closed in both ends of the well, we can expect a pressure jump (water hammer) at the bottom valve, and a pressure decrease at the well head. As shown Figure 7, the bottom pressure increase is close to 10 bar. The pressure decrease at the well head is smaller, since there is two-phase flow in the upper part of the well, which makes the fluid more compressible. The fluid column, which is in motion initially, will be compressed at the bottom and decompressed at the top. This will cause pressure waves that propagate up and down the well, which are slowly damped by friction. These pressure oscillations are clearly seen in Figure 7.

Figure 8 shows the temperature at three positions in the well. The temperature oscillations follow the pressure oscillations, since the fluid temperature is increased by compression.

Finally, Figure 9 shows the flow regimes during the shut-in. The bottom of the well has a dense/liquid phase column which stretches up to a depth of around 370 meters. At this depth, the liquid starts boiling, which leads to a layer of bubbly flow. Above this layer, the flow is predicted to be in a transition phase between bubbly flow and annular flow. These flow regimes are similar to what was observed by camera inspection in the Ketzin well during a shut-in [24]. In the upper part of the well, CO_2 was condensing and raining down on a layer of bubbly flow at around 300 meters depth. The amount of bubbles decreased with depth until a stationary single-phase liquid column was reached. Although the geothermal conditions in our simulations are different than those at Ketzin, the results are qualitatively similar.

6. Conclusion

We have presented a two-fluid model for flow of CO_2 in a vertical injection well, coupled with a model for heat conduction in the layers that comprise the well. The flow model predicts what flow regime the flow is in, and calculates friction and heat transfer accordingly. It was derived with emphasis on making sure that the mass transfer was continuous in the single-phase limit. The thermodynamic closure of the flow was provided by the Span-Wagner reference equation-of-state for CO_2.

The model was applied to sudden blowout and shut-in cases. The well was chosen to mimic the Sleipner CO_2 injection well, with similar well depth, geothermal gradient, reservoir temperature and reservoir pressure. The predicted temperature in the blowout case was not low enough to lead to

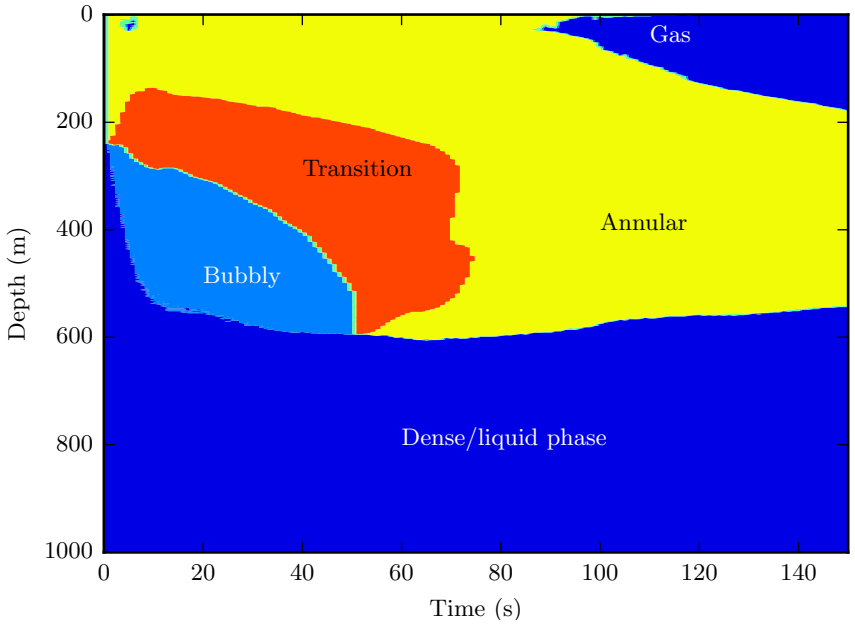

Figure 5: Flow regimes during blowout.

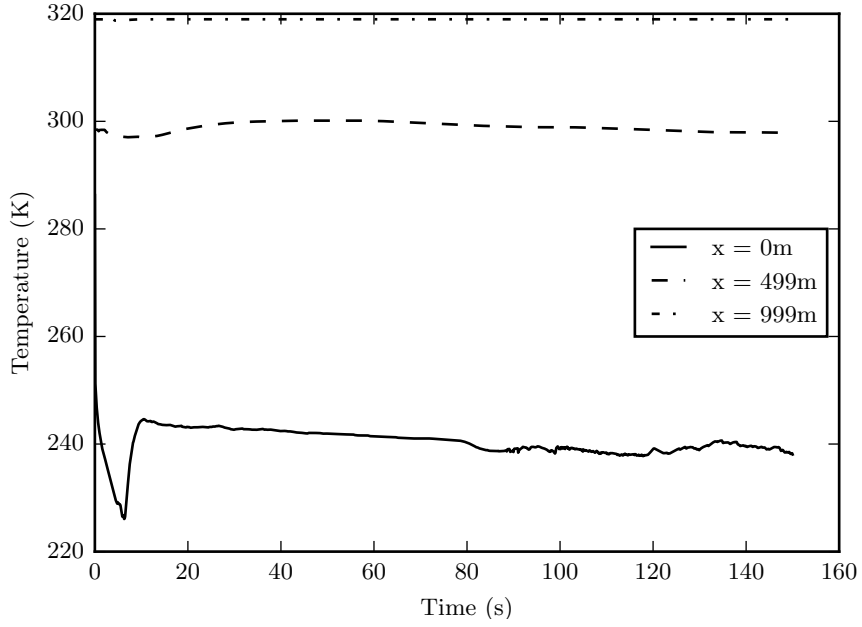

Figure 6: Temperature during blowout for three pipe locations.

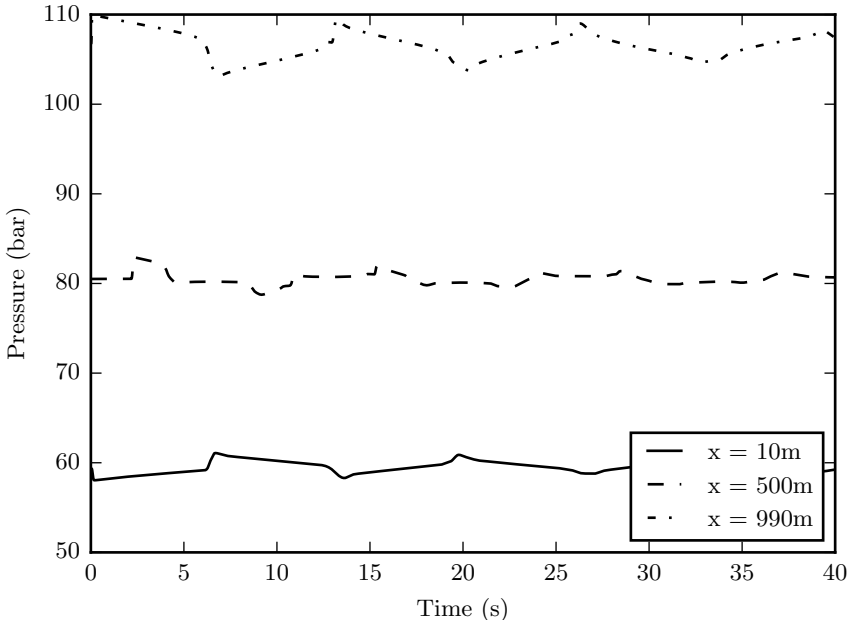

Figure 7: Pressure during shut-in at three pipe locations.

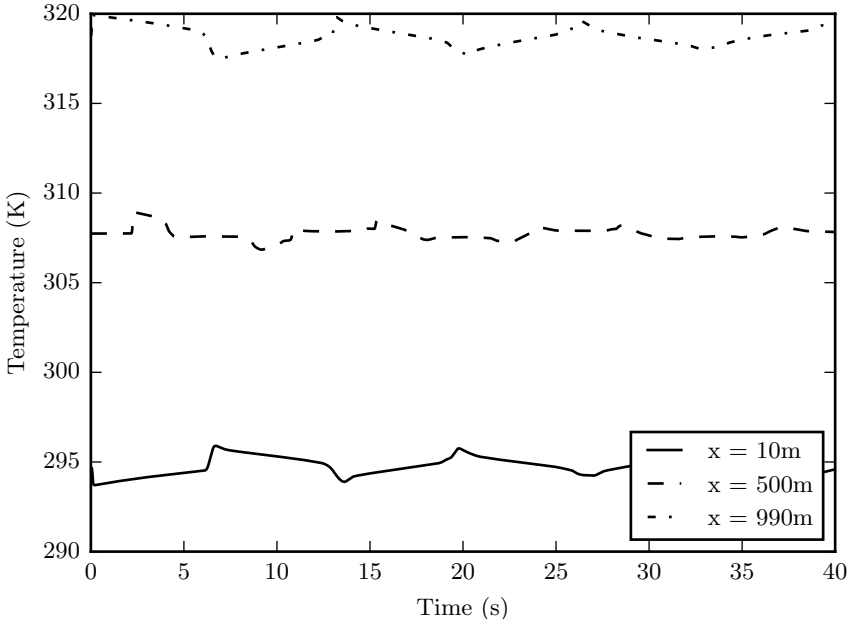

Figure 8: Temperature during shut-in at three pipe locations.

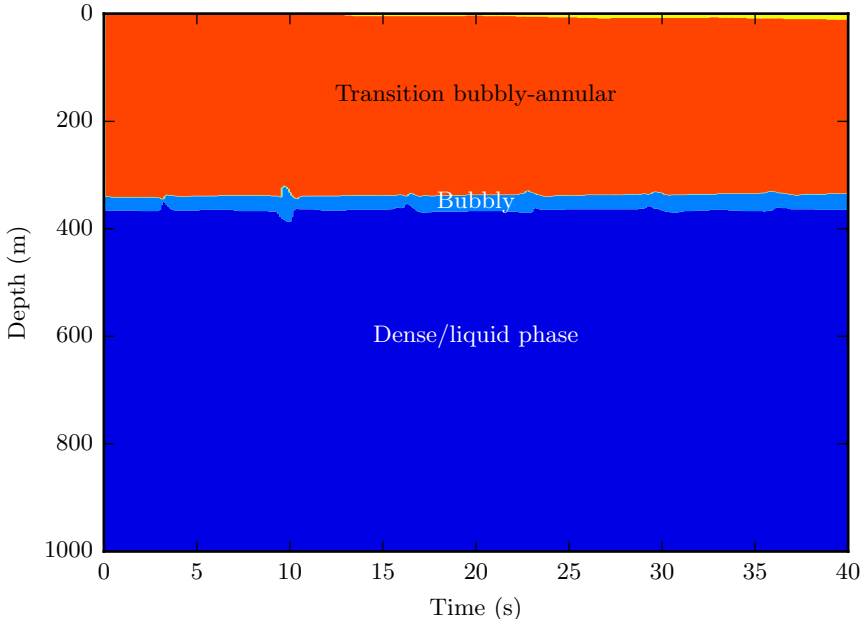

Figure 9: Flow regimes during shut-in.

dry ice in the well itself. Dry ice may nevertheless form as the flow exits the well head, but this is outside the modelled domain. The assumption that flow out of the reservoir is at the reservoir temperature leads to steady temperature conditions in the lower parts of the well, but this assumption disregards any Joule–Thomson effect that may occur in the reservoir. We also predicted that annular flow is prevalent where the flow is in a two-phase state.

In the shut-in case, we predicted the water hammer effect resulting from simultaneously closing well-head and bottom-hole valves when there is a steady downwards flow. With a flow rate similar to that in the Sleipner well, the bottom-hole pressure jump was predicted to be around 10 bar. The pressure then oscillates in ≈ 13 second cycles as the fluid is compressed and decompressed. The fluid is found to be in a single-phase state up to around 370 meters depth, above which the liquid starts to boil.

6.1. Further work

In further work, the model could be used to predict other transient operations of a well, such as shut-in on longer time scales, blowout with Joule–Thomson cooling in the reservoir, or intermittent injection from ships with resulting temperature variations. More realistic blowout and shut-in scenarios could also include valves that do not close or open suddenly, but are opened/closed over a certain time. The effect of a non-constant (time-dependent) injectivity, rather than a constant one used here, should also be considered. Moreover, horizontally deviating wells may behave differently due to e.g. different flow regimes, and could be worth looking into.

When it comes to applying the model for longer time scales (such as injection over several days/years), different numerical schemes are probably necessary to keep the computational cost at an acceptable level. For intermediate time scales, a semi-implicit scheme which solves pressure waves implicitly, could be used (see e.g. Chalons et al. [11], Evje and Flåtten [14]). For even longer time scales, the flow may be considered to be in a steady state, hence one can solve the steady-state ($\partial(\cdot)/\partial t = 0$) version of eqs. (1) to (5) using an ODE solver.

Currently, there is little available high resolution experimental data for CO_2 wells. If such data become available, a proper model validation could be performed to uncover potential modelling inaccuracies.

Acknowledgement

This publication has been produced in the *Ensuring well integrity during CO_2 injection* project and the *BIGCCS* Centre. The authors acknowledge the support of the following partners: ConocoPhillips, Gassco, Shell, Statoil, TOTAL, GDF SUEZ and the research programmes CLIMIT and Centres for environment-friendly energy (FME) of the Research Council of Norway (233893 and 193816). The first author acknowledges partial funding from the European Union's Horizon 2020 research and innovation programme under grant agreement No. 642976. We would also like thank our colleagues Eskil Aursand for contributions to the implementation of the Span–Wagner equation of state, Jonas Kjellstadli for implementing flow-regime correlations, and Morten Hammer and Alexandre Morin for discussions on the two-fluid model.

Appendix A. Nomenclature

Symbol	Description	Dimension	SI unit
A	Tubing cross-sectional area	L^2	m^2
a_k	Phase specific Heltmoltz free energy	L^2T^{-2}	$\mathrm{m}^2/\mathrm{s}^2$
c_p	Specific heat capacity at constant pressure	$L^2T^{-2}\Theta^{-1}$	$\mathrm{m}^2/(\mathrm{s}^2\,\mathrm{K})$
E	Total energy density	$ML^{-1}T^{-2}$	$\mathrm{kg}/(\mathrm{m}\,\mathrm{s}^2)$
e_k	Phase specific internal energy	L^2T^{-2}	$\mathrm{m}^2/\mathrm{s}^2$
E_k	Phase total energy density	$ML^{-1}T^{-2}$	$\mathrm{kg}/(\mathrm{m}\,\mathrm{s}^2)$
E_{kin}	Kinetic energy density	$ML^{-1}T^{-2}$	$\mathrm{kg}/(\mathrm{m}\,\mathrm{s}^2)$
f_{i}	Interface friction density	$ML^{-2}T^{-2}$	$\mathrm{kg}/(\mathrm{m}^2\,\mathrm{s}^2)$
$f_{\mathrm{wall},k}$	Phase wall friction density	$ML^{-2}T^{-2}$	$\mathrm{kg}/(\mathrm{m}^2\,\mathrm{s}^2)$
g_x	Gravity on well axis	LT^{-2}	m/s^2
I	Reservoir injectivity	LT	$\mathrm{m}\,\mathrm{s}$
$\mathcal{K}$	Mass transfer rate constant	L^2T^{-3}	$\mathrm{m}^2/\mathrm{s}^3$
M_k	Phase mass per total volume	ML^{-3}	kg/m^3
p	Pressure	$ML^{-1}T^{-2}$	$\mathrm{kg}/(\mathrm{m}\,\mathrm{s}^2)$
p_{i}	Interface pressure	$ML^{-1}T^{-2}$	$\mathrm{kg}/(\mathrm{m}\,\mathrm{s}^2)$
Q	Heat transfer	$ML^{-1}T^{-3}$	$\mathrm{kg}/(\mathrm{m}\,\mathrm{s}^3)$
r	Radius from tubing centre	L	m
R	Specific gas constant	$L^2T^{-2}\Theta^{-1}$	$\mathrm{m}^2/(\mathrm{s}^2\,\mathrm{K})$
S	Volumetric entropy	$ML^{-1}T^{-2}\Theta^{-1}$	$\mathrm{kg}/(\mathrm{m}\,\mathrm{s}^2\,\mathrm{K})$
t	Time	T	s
v_k	Phase velocity	LT^{-1}	m/s
v_{i}	Interface velocity	LT^{-1}	m/s
$\hat{v}$	Centre-of-mass velocity	LT^{-1}	m/s
$\bar{v}$	Volume-averaged velocity	LT^{-1}	m/s
x	Distance along well	L	m
α_k	Phase volume fraction	–	–
δ	Regularizing pressure factor	–	–
κ	Thermal conductivity	$MLT^{-1}\Theta^{-1}$	$\mathrm{kg}\,\mathrm{m}/(\mathrm{s}\,\mathrm{K})$
μ_k	Phase specific Gibbs free energy	L^2T^{-2}	$\mathrm{m}^2/\mathrm{s}^2$
Π_k	Phase momentum per total volume	$ML^{-2}T^{-1}$	$\mathrm{kg}/(\mathrm{m}^2\,\mathrm{s})$
ρ	Mixture mass density	ML^{-3}	kg/m^3
ρ_k	Phase mass density	ML^{-3}	kg/m^3
Ψ	Mass density transfer rate	$ML^{-3}T^{-1}$	$\mathrm{kg}/(\mathrm{m}^3\,\mathrm{s})$

References

[1] A. Albawi. Influence of thermal cycling on cement sheath integrity. Master's thesis, Norwegian University of Science and Technology, Faculty of Engineering Science and Technology, Department of Petroleum Engineering and Applied Geophysics, 2013.

[2] L. André, P. Audigane, M. Azaroual, and A. Menjoz. Numerical modeling of fluid–rock chemical interactions at the supercritical CO_2-liquid interface during CO_2 injection into a carbonate reservoir, the Dogger aquifer (Paris basin, France). *Energy Conversion and Management*, 48(6):1782 – 1797, 2007. ISSN 0196-8904. doi: 10.1016/j.enconman.2007.01.006. Geologic Carbon Sequestration and Methane Hydrates Research from the TOUGH Symposium 2006.

[3] A. Austegard, E. Solbraa, G. De Koeijer, and M. J. Mølnvik. Thermodynamic models for calculating mutual solubilities in H_2O-CO_2-CH_4 mixtures. *Chemical Engingeering Research & Design*, 84(A9):781–794, Sept. 2006. doi:10.1205/cherd05023.

[4] M. Azaroual, L. Andre, Y. Peysson, J. Pironon, D. Broseta, F. Dedecker, P. Egermann, J. Desroches, and J. Hy-Billiot. Behavior of the CO_2 injection well and the near wellbore during carbon dioxide injection in saline aquifers. In *Proceedings, TOUGH Symposium*, 2012.

[5] M. Baer and J. Nunziato. A two-phase mixture theory for the deflagration-to-detonation transition (DDT) in reactive granular materials. *International journal of multiphase flow*, 12(6):861–889, 1986.

[6] M. Baudin, C. Berthon, F. Coquel, R. Masson, and Q. H. Tran. A relaxation method for two-phase flow models with hydrodynamic closure law. *Numerische Mathematik*, 99(3):411–440, Jan. 2005.

[7] K. H. Bendiksen, D. Malnes, R. Moe, and S. Nuland. The dynamic two-fluid model OLGA: Theory and application. *SPE Production Engineering*, 6(2):171–180, May 1991. doi:10.2118/19451-PA.

[8] D. Bestion. The physical closure laws in the CATHARE code. *Nuclear Engineering and Design*, 124(3):229–245, Dec. 1990. doi:10.1016/0029-5493(90)90294-8.

[9] K. S. Bjørkevoll. (SINTEF Petroleum) Personal communication, 2014.

[10] J. R. Cannon. *The One-Dimensional Heat Equation*. Encyclopedia of Mathematics and its Applications. Cambridge University Press, 1984. ISBN 9780521302432.

[11] C. Chalons, F. Coquel, S. Kokh, and N. Spillane. Large Time-Step Numerical Scheme for the Seven-Equation Model of Compressible Two-Phase Flows. In Fort, J and Furst, J and Halama, J and Herbin, R and Hubert, F, editor, *FINITE VOLUMES FOR COMPLEX APPLICATIONS VI: PROBLEMS & PERSPECTIVES, VOLS 1 AND 2*, volume 4 of *Springer Proceedings in Mathematics*, pages 225–233. CMLA ENS Cachan; IFP Energies Nouvelles; IRSN; LATP Univ Aix Marseille I; MOMAS Grp; Univ Paris XIII; Univ Paris Est Marne Vallee; Univ Pierre & Marie Curie, 2011. ISBN 978-3-642-20671-9. doi:10.1007/978-3-642-20671-9_24. 6th International Symposium on Finite Volumes for Complex Applications, Prague, CZECH REPUBLIC, JUN 06-10, 2011.

[12] J. C. Chen. Correlation for boiling heat transfer to saturated fluids in convective flow. *Industrial & Engineering Chemistry Process Design and Development*, 5 (3):322–329, 1966. doi:10.1021/i260019a023.

[13] F. W. Dittus and L. M. K. Boelter. Heat transfer in automobile radiators of the tubular type. *University of California publications in engineering*, 2:443–461, 1930.

[14] S. Evje and T. Flåtten. Weakly implicit numerical schemes for a two-fluid model. *SIAM JOURNAL ON SCIENTIFIC COMPUTING*, 26(5):1449–1484, 2005.

[15] T. Flåtten and H. Lund. Relaxation two-phase flow models and the subcharacteristic condition. *Mathematical Models and Methods in Applied Sciences*, 21(12): 2379–2407, Dec. 2011. doi:10.1142/S0218202511005775.

[16] T. Flåtten, A. Morin, and S. T. Munkejord. Wave propagation in multicomponent flow models. *SIAM Journal on Applied Mathematics*, 70(8):2861–2882, Sept. 2010. doi:10.1137/090777700.

[17] H. K. Forster and N. Zuber. Dynamics of vapor bubbles and boiling heat transfer. *AIChE Journal*, 1(4):531–535, 1955. ISSN 1547-5905. doi:10.1002/aic.690010425.

[18] S. Goodarzi, A. Settari, M. D. Zoback, D. Keith, et al. Thermal aspects of geomechanics and induced fracturing in CO_2 injection with application to CO_2 sequestration in Ohio River Valley. In *SPE International Conference on CO_2 Capture, Storage, and Utilization*. Society of Petroleum Engineers, 2010.

[19] Halliburton. N-SOLATE® High Performance Insulating Packer Fluids, 2012. URL `http://www.halliburton.com/public/bar/contents/Data_Sheets/web/Sales_Data_Sheets/H05923.pdf`. [Online; accessed 29 September 2014].

[20] M. Hammer and A. Morin. A method for simulating two-phase pipe flow with real equations of state. *Computers & Fluids*, 100(0):45–58, 2014. ISSN 0045-7930. doi:10.1016/j.compfluid.2014.04.030.

[21] M. Hammer, Å. Ervik, and S. T. Munkejord. Method using a density–energy state function with a reference equation of state for fluid-dynamics simulation of vapor–liquid–solid carbon dioxide. *Industrial & Engineering Chemistry Research*, 52(29):9965–9978, 2013.

[22] W. Han, K.-Y. Kim, M. Lu, B. McPherson, C. Lu, and S.-Y. Lee. Injectivity changes and associated temperature disequilibrium: Numerical study. *Energy Procedia*, 4(0):4552 – 4558, 2011. ISSN 1876-6102. doi: 10.1016/j.egypro.2011.02.413. 10th International Conference on Greenhouse Gas Control Technologies.

[23] O. Hansen, D. Gilding, B. Nazarian, B. Osdal, P. Ringrose, J.-B. Kristoffersen, O. Eiken, and H. Hansen. Snøhvit: The history of injecting and storing 1 Mt CO_2 in the fluvial Tubåen fm. *Energy Procedia*, 37:3565–3573, 2013. ISSN 1876-6102. doi: 10.1016/j.egypro.2013.06.249. GHGT-11.

[24] J. Henninges, A. Liebscher, A. Bannach, W. Brandt, S. Hurter, S. Köhler, and F. Möller. P-T-ρ and two-phase fluid conditions with inverted density profile in observation wells at the CO_2 storage site at Ketzin (Germany). *Energy Procedia*, 4(0):6085–6090, 2011. ISSN 1876-6102. doi:10.1016/j.egypro.2011.02.614. 10th International Conference on Greenhouse Gas Control Technologies.

[25] IEA. *Energy Technology Perspectives*. 2014. ISBN 978-92-64-20801-8. doi:10.1787/energy_tech-2014-en.

[26] K. Karlsen, C. Klingenberg, and N. Risebro. A relaxation scheme for conservation laws with a discontinuous coefficient. *Mathematics of computation*, 73(247):1235–1259, 2004.

[27] J. Kjärstad, R. Skagestad, N. H. Eldrup, and F. Johnsson. Transport of CO_2 in the nordic region. *Energy Procedia*, 63:2683–2690, 2014. ISSN 1876-6102. doi:10.1016/j.egypro.2014.11.290. 12th International Conference on Greenhouse Gas Control Technologies, GHGT-12.

[28] L. Klinkby, C. M. Nielsen, E. Krogh, I. E. Smith, B. Palm, and C. Bernstone. Simulating rapidly fluctuating CO_2 flow into the Vedsted CO_2 pipeline, injection well and reservoir. *Energy Procedia*, 4(0):4291 – 4298, 2011. ISSN 1876-6102. doi:10.1016/j.egypro.2011.02.379. 10th International Conference on Greenhouse Gas Control Technologies.

[29] E. Krogh, R. Nilsen, and R. Henningsen. Liquefied CO_2 injection modelling. *Energy Procedia*, 23(0):527–555, 2012. ISSN 1876-6102. doi:10.1016/j.egypro.2012.06.022. The 6th Trondheim Conference on CO_2 Capture, Transport and Storage.

[30] R. J. LeVeque. *Finite Volume Methods for Hyperbolic Problems*. Cambridge University Press, Cambridge, UK, 2002. ISBN 0-521-00924-3.

[31] X. Li, R. Xu, L. Wei, and P. Jiang. Modeling of wellbore dynamics of a CO_2 injector during transient well shut-in and start-up operations. *International Journal of Greenhouse Gas Control*, 42:602–614, 2015. ISSN 1750-5836. doi:10.1016/j.ijggc.2015.09.016.

[32] E. Lindeberg. Modelling pressure and temperature profile in a CO_2 injection well. *Energy Procedia*, 4(0):3935–3941, 2011. ISSN 1876-6102. doi:10.1016/j.egypro.2011.02.332. 10th International Conference on Greenhouse Gas Control Technologies.

[33] G. Linga. A hierarchy of non-equilibrium two-phase flow models. *Submitted*. Available online at `http://folk.ntnu.no/gautelin/pub/twofluid.pdf`, 2015.

[34] G. Linga, P. Aursand, and T. Flåtten. Two-phase nozzle flow and the subcharacteristic condition. *Journal of Mathematical Analysis and Applications*, 426(2):917–934, 2015.

[35] M. Lu and L. D. Connell. Non-isothermal flow of carbon dioxide in injection wells during geological storage. *International Journal of Greenhouse Gas Control*, 2(2):248–258, 2008. ISSN 1750-5836. doi:10.1016/S1750-5836(07)00114-4.

[36] M. Lu and L. D. Connell. Transient, thermal wellbore flow of multispecies carbon dioxide mixtures with phase transition during geological storage. *International Journal of Multiphase Flow*, 63:82–92, 2014. doi:10.1016/j.ijmultiphaseflow.2014.04.002.

[37] M. Lu and L. D. Connell. The transient behaviour of CO_2 flow with phase transition in injection wells during geological storage – Application to a case study. *Journal of Petroleum Science and Engineering*, 124:7–18, 2014. doi:10.1016/j.petrol.2014.09.024.

[38] H. Lund. A hierarchy of relaxation models for two-phase flow. *SIAM Journal on Applied Mathematics*, 72 (6):1713–1741, Dec. 2012. doi:10.1137/12086368X.

[39] H. Lund, M. Torsæter, and S. T. Munkejord. Study of thermal variations in wells during CO_2 injection. In *SPE Bergen One Day Seminar*, Bergen, Norway, Apr. 2015. Society of Petroleum Engineers. doi:10.2118/173864-MS. Paper SPE-173864-MS.

[40] P. J. Martínez Ferrer, T. Flåtten, and S. T. Munkejord. On the effect of temperature and velocity relaxation in two-phase flow models. *ESAIM: Mathematical Modelling and Numerical Analysis*, 46(2):411–442, Mar. 2012. doi:10.1051/m2an/2011039.

[41] J. M. Masella, Q. H. Tran, D. Ferre, and C. Pauchon. Transient simulation of two-phase flows in pipes. *International Journal of Multiphase Flow*, 24(5):739–755, Aug. 1998.

[42] A. Morin and T. Flåtten. A two-fluid four-equation model with instantaneous thermodynamical equilibrium. *ESAIM: M2AN*, 2015. To appear.

[43] S. T. Munkejord and M. Hammer. Depressurization of CO_2-rich mixtures in pipes: Two-phase flow modelling and comparison with experiments. *International Journal of Greenhouse Gas Control*, 37:398–411, June 2015. doi:10.1016/j.ijggc.2015.03.029.

[44] S. T. Munkejord, S. Evje, and T. Flåtten. A MUSTA scheme for a nonconservative two-fluid model. *SIAM Journal on Scientific Computing*, 31(4):2587–2622, June 2009. doi:10.1137/080719273.

[45] R. Natalini. Recent results on hyperbolic relaxation problems. analysis of systems of conservation laws. *Chapman & Hall/CRC Monographs and Surveys in Pure and Applied Mathematics*, 99:128–198, 1997.

[46] J. M. Nordbotten and M. A. Celia. *Geological storage of CO_2: Modeling approaches for large-scale simulation*. John Wiley & Sons, 2011.

[47] J. M. Nordbotten, M. A. Celia, and S. Bachu. Injection and storage of CO_2 in deep saline aquifers: Analytical solution for CO_2 plume evolution during injection. *Transport in Porous media*, 58(3):339–360, 2005.

[48] J. M. Nordbotten, M. A. Celia, S. Bachu, and H. K. Dahle. Semianalytical solution for CO_2 leakage through an abandoned well. *Environmental science & technology*, 39(2):602–611, 2005.

[49] H. Paillère, C. Corre, and J. R. García Cascales. On the extension of the AUSM+ scheme to compressible two-fluid models. *Computers & Fluids*, 32(6):891–916, July 2003. doi:10.1016/S0045-7930(02)00021-X.

[50] L. Pan, C. M. Oldenburg, Y.-S. Wu, and K. Pruess. Wellbore flow model for carbon dioxide and brine. *Energy Procedia*, 1(1):71–78, 2009. ISSN 1876-6102. doi:10.1016/j.egypro.2009.01.012. Proceedings of the 9th International Conference on Greenhouse Gas Control Technologies (GHGT-9), 16–20 November 2008, Washington DC, USA.

[51] L. Pan, S. W. Webb, and C. M. Oldenburg. Analytical solution for two-phase flow in a wellbore using the drift-flux model. *Advances in Water Resources*, 34(12):1656–1665, 2011. ISSN 0309-1708. doi:10.1016/j.advwatres.2011.08.009.

[52] L. Pareschi and G. Russo. Implicit-explicit Runge–Kutta schemes and applications to hyperbolic systems with relaxation. *Journal of Scientific Computing*, 25:129–155, 2005.

[53] M. Pelanti and K.-M. Shyue. A mixture-energy-consistent six-equation two-phase numerical model for fluids with interfaces, cavitation and evaporation waves. *Journal of Computational Physics*, 259:331–357, 2014.

[54] V. H. Ransom et al. *RELAP5/MOD3 Code Manual, NUREG/CR-5535*. Idaho National Engineering Laboratory, ID, 1995.

[55] S. Roussanaly, A. L. Brunsvold, and E. S. Hognes. Benchmarking of CO_2 transport technologies: Part II – Offshore pipeline and shipping to an offshore site. *International Journal of Greenhouse Gas Control*, 28:283–299, 2014.

[56] B. Ruan, R. Xu, L. Wei, X. Ouyang, F. Luo, and

P. Jiang. Flow and thermal modeling of CO_2 in injection well during geological sequestration. *International Journal of Greenhouse Gas Control*, 19(0):271–280, 2013.

[57] R. Saurel and R. Abgrall. A multiphase Godunov method for compressible multifluid and multiphase flow. *Journal of Computational Physics*, 150(2):425–467, Apr. 1999.

[58] R. Saurel, F. Petitpas, and R. Abgrall. Modelling phase transition in metastable liquids: application to cavitating and flashing flows. *Journal of Fluid Mechanics*, 607: 313–350, July 2008. doi:10.1017/S0022112008002061.

[59] A. Singhe, J. Ursin, J. Henninges, G. Pusch, and L. Ganzer. Modeling of temperature effects in CO_2 injection wells. *Energy Procedia*, 37(0):3927–3935, 2013. ISSN 1876-6102. doi:10.1016/j.egypro.2013.06.291. GHGT-11.

[60] S. Solem, P. Aursand, and T. Flåtten. Wave dynamics of linear hyperbolic relaxation systems. *Journal of Hyperbolic Differential Equations*, 12(04):655–670, 2015. doi:10.1142/S0219891615500186.

[61] R. Span and W. Wagner. A new equation of state for carbon dioxide covering the fluid region from the triple-point temperature to 1100 K at pressures up to 800 MPa. *Journal of Physical and Chemical Reference Data*, 25(6):1509–1596, 1996.

[62] H. B. Stewart and B. Wendroff. Two-phase flow: Models and methods. *Journal of Computational Physics*, 56(3): 363–409, 1984.

[63] G. Strang. On the construction and comparison of difference schemes. *SIAM Journal on Numerical Analysis*, 5(3):506–517, 1968.

[64] J. H. Stuhmiller. The influence of interfacial pressure forces on the character of two-phase flow model equations. *International Journal of Multiphase Flow*, 3(6): 551–560, Dec. 1977. doi:10.1016/0301-9322(77)90029-5.

[65] E. S. Thu. Modeling of transient CO_2 flow in pipelines and wells. Master's thesis, Norwegian University of Science and Technology, 2013.

[66] I. Tiselj, G. **C**erne, A. Horvat, J. Gale, I. Parzer, M. Giot, J. Seynhaeve, B. Kucienska, and H. Lemonnier. *WAHA3 code manual*, 2004. JSI Report IJS-DP-8841, Jo**z**ef Stefan Insitute, Ljubljana, Slovenia.

[67] I. Toumi. An upwind numerical method for two-fluid two-phase flow models. *Nuclear Science and Engineering*, 123(2):147–168, 1996.

[68] T. N. Vermeulen. Knowledge sharing report - CO_2 liquid logistics shipping concept (LLSC): Overall supply chain optimization. Technical report, Global CCS Institute, Anthony Veder, Vopak, June 2011.

[69] N. Zuber and J. A. Findlay. Average volumetric concentration in two-phase flow systems. *Journal of Heat Transfer – Transactions of the ASME*, 87:453–468, Nov. 1965.